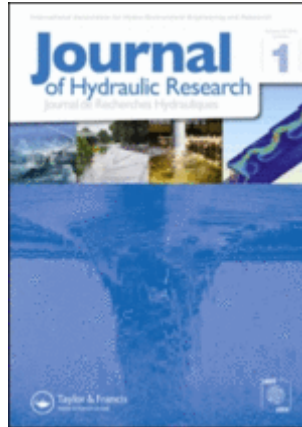


This Manuscript has been submitted for publication in the Journal of Hydraulics Research. This manuscript is currently under peer review and still needs to be formally accepted for publication. Further versions might slightly change from the present one. The final version will be available via the 'Peer-reviewed Publication DOI link' on the right-hand side of the webpage. Please feel free to contact the authors.



Finite volumes methods for coupled surface-subsurface flows

Journal:	<i>Journal of Hydraulic Research</i>
Manuscript ID	TJHR-2023-0011
Manuscript Type:	Research paper
Date Submitted by the Author:	05-Feb-2023
Complete List of Authors:	Delpierre, Nathan; UCLouvain, IMMC - Civil and Environmental Engineering Soares-Frazao, Sandra; UCLouvain, iMMC - Civil and Environmental Engineering Rattez, Hadrien; UCLouvain, IMMC - Civil and Environmental Engineering
Keywords:	shallow-water equations, finite volume, embankment, numerical simulation, overtopping flows, Richards equation
JHR Keywords:	Groundwater/surface water interaction < Environmental Fluid Mechanics, Flows through porous media, Hydraulic structure design & management < Applied fluid mechanics and hydraulic engineering, Interactions with surfaces < Multiphase and stratified flows

SCHOLARONE™
Manuscripts

Finite volumes methods for coupled surface-subsurface flows

NATHAN DELPIERRE, PhD student, *Institute of Mechanics, Materials and Civil Engineering, UCLouvain, Louvain-la-Neuve, Belgium*

Email: nathan.delpierre@uclouvain.be

HADRIEN RATTEZ, Professor, *Institute of Mechanics, Materials and Civil Engineering, UCLouvain, Louvain-la-Neuve, Belgium*

Email: hadrien.rattez@uclouvain.be

SANDRA SOARES-FRAZAO (IAHR Member), Professor, *Institute of Mechanics, Materials and Civil Engineering, UCLouvain, Louvain-la-Neuve, Belgium*

Email: Sandra.soares-frazao@uclouvain.be (author for correspondence)

Running Head (i.e. the text that appears in the top margin of the published page): provide a short title here (up to seven words).

Earthen embankments: coupled surface and sub-surface flows

Finite volumes methods for coupled surface-subsurface flows

ABSTRACT

Earthen embankments are subject to increasing threats because of climate change inducing sequences of severe drought periods followed by floods possibly leading to overtopping of the structures. Consequently, the water saturation of the dike can vary significantly both in space and time, and the resulting groundwater flow can affect the free-surface flow in case of overtopping. Conversely, the free-surface flow can modify the pore water content, which controls erosion and slope instabilities. In this paper, a combined approach to such situations is presented, in which the degree of saturation and the flow through the embankment are simulated by solving the two-dimensional Richards equation on an unstructured mesh with an implicit finite volume scheme that is coupled to the system of shallow-water equations solved in one dimension using an explicit finite-volume scheme. The coupled model is validated on several situations of flows through and over earthen embankments with different constitutive materials.

Keywords: Richards equation, shallow-water equations, overtopping flows, finite volume, embankment, numerical simulation.

1 Introduction

In the current context of climate change and aging infrastructures, breaching of earthen embankments becomes a key issue. Dikes have an essential protective role in flood defence, coastal protection or for the storage of waste from the mining industry. Sea-level rise, increased extreme precipitations and drought events (IPCC, 2021) have put additional stress on water control structures such as dikes. Failure of these structures may present a high risk for stakeholders and neighboring communities, and devastating consequences such as human life losses, material or environmental damages. Recent examples include the environmental disaster in Brumadinho (Brazil, 2019) where a tailings dam failed causing 259 casualties, the levee failures in New Orleans (2005) leaving the city completely flooded for several days or the recent intense rainfall of July 2021 causing dike failures in the Netherlands and Belgium (Meersen in South Limburg, Herk-de-Stad in Limburg). Analyses of previous events have shown that overtopping is the main cause of failure (Foster et al., 2000). This phenomenon is complex, combining fast erosive flow over the dike with seepage through the dike. Flow through the dike can lead to internal erosion, but also modifies the water saturation level inside the embankment affecting the breaching initiation and the pace towards complete failure when combined to overtopping. This internal flow is highly dependent on the initial saturation of the dike material, whose effects on the failure have been largely overlooked so far. However, at full saturation, cohesion of the dike material is greatly reduced, and thus the dike strength. To avoid such situations, drains are often placed in the dike at its downstream part to control the saturation profile by lowering the level of the water table in the dike and therefore increasing the time required for the full saturation. Therefore, a better understanding of the combination of the initial dike saturation with the overtopping flow and the internal flow will therefore fill a

1
2
3 knowledge gap with the ambition to provide a physically based model that can be used to reduce
4 the risks associated with these phenomena.
5
6

7 Many numerical models have been developed to design or assess the risk of failure of existing
8 embankments when they are submitted to overtopping or internal flows. Most of these models
9 allow to consider only the overtopping flow, by solving the shallow water equations (Shiach et
10 al. 2004, Shao et al. 2006, Van Emelen et al., 2016), or the internal flow inside the pores of the
11 embankment by solving the Richards equation (Tsai et al. 2008, Chávez-Negrete et al. 2018).
12 For this latter equation, in most cases, the numerical resolution is performed either by finite
13 elements, finite volumes or finite differences, implying different types of spatial discretization
14 (Farthing & Ogden, 2017), using generally structured meshes. From the temporal point of view,
15 most models use an implicit time discretization (Farthing & Ogden, 2017), because of the
16 inability of the explicit formulations to solve the problem when the soil is saturated (Caviedes-
17 Voullième et al., 2013).
18
19
20
21
22
23
24
25

26 Coupled models considering the interaction between subsurface and surface water flows exist
27 in the literature but they are mostly used to understand the processes of irrigation or watershed
28 replenishment (Furman 2008, Weill et al. 2009). Moreover, these models tend to focus on
29 variables such as water content and infiltration, rather than pore pressure which is of interest in
30 case of embankment stability issues. Therefore, coupled models are still not widespread in the
31 engineering community for solving practical field cases, and decoupled models are often
32 preferred where the focus is set on one of the models, i.e. overtopping flow or infiltration, while
33 the second one is solved with empirical parameters or functions (Furman, 2008). Indeed,
34 solving the coupled problem accurately in a comprehensive way poses several challenges,
35 including changing boundary conditions as the soil can be submerged or not and these
36 conditions may change over time, resulting in possible mass conservation errors linked to the
37 numerical schemes used.
38
39
40
41
42
43
44
45

46 Different numerical methods have been proposed to address these challenges and simulate
47 hydrostatic surface-subsurface flows. Casulli (2017) presented a method that uses a vertically
48 integrated continuity equation, which is based on the principles of the Richards and Navier-
49 Stokes equations on an orthogonal unstructured grid. An algorithm, based on the Darcy law,
50 was used to solve the groundwater flow in the saturated case considering purely hydrostatic
51 flow. Similarly, De Maet and Hanert (2011) proposed an explicit solver for the Richards
52 equation in the unsaturated zone, but uses a method called the “false transient method” to handle
53 the case when soil becomes saturated because of the explicit solver being unable to handle the
54 saturated case. Additionally, Caviedes-Voullième et al. (2012) presented an algorithm that
55
56
57
58
59
60

employs a non-iterative external coupling algorithm, using the 2D shallow-water equation for surface flows and the 3D Richards equation for subsurface flows on structured meshes. Finally, Mizutani et al. (2013) proposed a coupled solver that was used to study the influence of soil saturation on a dike's overtopping flow using a bi-dimensional structured mesh.

The aim of the present article is therefore to present a coupled finite-volume numerical model of both flows over and through earthen dikes using unstructured meshes and ensuring mass conservation, featuring a robust coupling between the two types of flows. The study is essentially divided into three parts: (i) the development and validation of an implicit Richards equation solver using finite volumes on unstructured meshes for simulating the movement of water in unsaturated and saturated soils, (ii) the coupling of both models and a first validation on academic cases, and (iii) the application on complex cases to highlight the performances of the new scheme.

2 Finite-volume resolution of the Richards equations

2.1 Richards equation and model closure

The Richards equation (Richards, 1931) is a nonlinear partial differential equation describing the transfer of water in unsaturated soils under non-permanent conditions. It is based on the combination of the continuity equation and the Darcy equation.

Let Ω be the bidimensional domain, $\partial\Omega$ its boundary and \mathbf{n} the normal vector at the boundary pointing outwards. The Richards's equation can be written, in its mixed form, as:

$$\frac{\partial \theta(h)}{\partial t} - \nabla \cdot [K(h) \nabla (h + z)] = 0 \quad (1)$$

Where $\theta(-)$ is the volumetric water content, $h(\mathbf{x}, t)$ (cm) the pressure head and K the hydraulic conductivity ($\text{cm}\cdot\text{s}^{-1}$). One of the main difficulties of the Richards equation lies in its non-linearity caused by the relationships between the volumetric water content, the pressure head and the hydraulic conductivity. Multiple models exist in order to describe the relations between those variables, but the most frequent one is the Mualem-van Genuchten model (1980), used in this work. The latter was developed in order to facilitate the representation of the so-called soil-water retention curve (SWRC) that links volumetric water content and pressure head. The development of this model follows the difficulty of determining the hydraulic conductivity in the case of unsaturated soils. While the experimental determination of the hydraulic conductivity is relatively simple in the case of a saturated soil, the hydraulic conductivity in an unsaturated soil is more difficult to determine because of its dependency on many factors. Moreover, its extensive measurement is expensive and time consuming as it usually requires the use of different methodologies to determine its evolution for various ranges of pressure.

The Mualem-van Genuchten model allows a smooth transitioning between the unsaturated and the saturated state of the soil with the following relationships:

$$\theta = \begin{cases} \frac{\theta_s - \theta_r}{\left(1 + (\alpha|h|)^\eta\right)^\mu} + \theta_r & \text{if } h \leq 0 \\ \theta_s & \text{if } h > 0 \end{cases} \quad (2)$$

$$S_e = \frac{\theta - \theta_r}{\theta_s - \theta_r} \quad (3)$$

$$K = \begin{cases} K_s S_e^L \left[1 - (1 - S_e^{1/\mu})^\mu\right]^2 & \text{if } h \leq 0 \\ K_s & \text{if } h > 0 \end{cases} \quad (4)$$

$$C = \begin{cases} -\mu\eta\alpha^\eta \frac{\theta_s - \theta_r}{\left(1 + \alpha^\eta |h|^\eta\right)^{\mu+1}} |h|^\eta h^{-1} & \text{if } h \leq 0 \\ 0 & \text{if } h > 0 \end{cases} \quad (5)$$

$$\mu = 1 - \frac{1}{\eta} \quad (6)$$

Where θ_s is the saturated volumetric water content (-), θ_r the residual volumetric water content (-), S_e the equivalent volumetric water content (-), K_s the saturated hydraulic conductivity and C the hydraulic capacity (cm^{-1}) which represents the volumetric water content variation due to a head pressure variation ($\partial\theta/\partial h$).

The other parameters in equations (2-6) need to be calibrated using laboratory measurements. Still, some of those have a physical meaning and can be obtained using closure relations. For example, η is linked to the pore pressure distribution and describes the slope of the curve (Mualem, 1976). Some authors (e.g. Caviedes-Voullième et al., 2013; Soltani et al., 2021) suggest that the α parameter is related to the air-entry pressure h_e . This pressure is defined (Brooks and Corey, 1964) as the pressure state where the entry of air (and thus the evacuation of water) into the largest pore becomes possible during the desaturation process of a saturated soil. This pressure can be found graphically by crossing the horizontal asymptote at $\theta = \theta_s$ with the tangent to the SWRC (Benson et al., 2014).

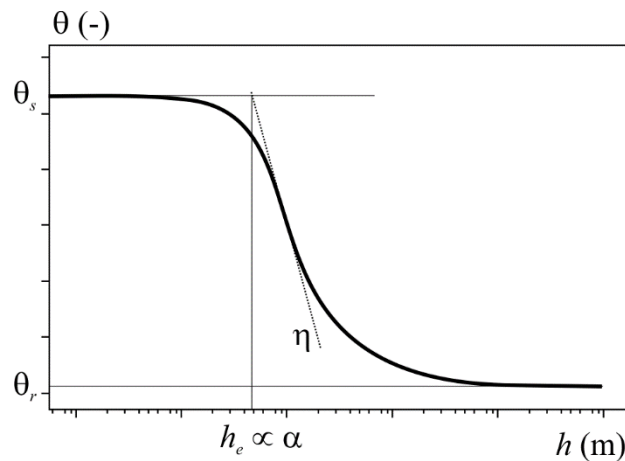


Figure 1 Schematic representation of the soil-water retention curve

Soltani et al. (2021) highlight the fact that a wrong evaluation of this parameter leads to a very bad evaluation of assessment of the water content, which is directly related to the relative permeability of the soil but also to its weight and shear strength.

2.2 Unstructured finites volume resolution

An implicit Eulerian solver is employed in this work in which a system of equations is solved until convergence for each time step:

$$\mathbf{A}_{i,j} \mathbf{h}_j^{n+1,m+1} = \mathbf{c}_i \quad (7)$$

where \mathbf{A} is a square matrix of n by n elements containing terms calculated with the spatial and temporal integrations at time $n + 1$, but at iteration step m ; \mathbf{h} is the vector of unknowns pressure heads and \mathbf{c} the vector of external source terms:

$$\mathbf{A}_{i,i} = \frac{c_i^{n+1,m}}{\Delta t} \Omega_i + \sum_k K_{i,k} L_{i,k} d_{i,k}^{-1} \quad (8)$$

$$\mathbf{A}_{i,j} = -K_{i,j} L_{i,j} d_{i,j}^{-1} \quad (9)$$

$$\mathbf{c}_i = \sum_k K_{i,k} L_{i,k} (n_z)_{i,k} + \frac{\Omega_i}{\Delta t} (\theta_i^{n,m} - \theta_i^{n+1,m} + C_i^{n+1,m} h_i^{n+1,m}) \quad (10)$$

Other terms than those presented previously include: Δt the time step (s), Ω_i the area of the computational cell (m^2), $K_{i,j}$ the hydraulic conductivity at the interface between two cells, $L_{i,j}$ the length of the edge (m) and $d_{i,j}$ the distance between the centers of the two adjacent cells (m), $(n_z)_{i,j}$ the outgoing z-axis pointing normal to the interface between two computational cells (Figure 2).

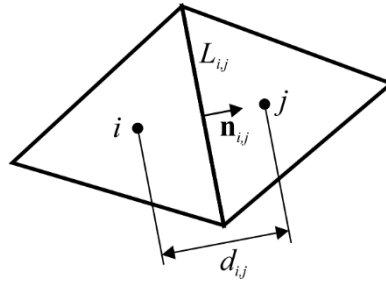


Figure 2 Computational cells for the Richards equation, definition of variables.

2.3 Validation

Two classical benchmarks are used for the validation of the Richards equation solver, consisting in flows through a column of unsaturated soil: first the drainage of a soil column, and then the propagation of a sharp infiltration front.

The soil characteristics used for both tests are presented in Table 1. These soil data were presented at first in a work by Celia et al. (1990) and the soil samples were collected in New Mexico. Since then, these soil data have been used in several studies to validate various Richard's solvers (Kavetski et al., 2001; Caviedes-Voullième et al., 2013; Su et al., 2022).

Table 1 Soil parameters for the test cases

Parameter	Value	Unit	Parameter	Value	Units
K_s	0.00922	cm s ⁻¹	α	0.0335	cm s ⁻¹
θ_r	0.102	-	$\hat{\eta}$	2	-
θ_s	0.368	-	\hat{L}	0.5	-

Drainage of soil column

Caviedes-Voullième et al. (2013) proposed an idealized academic test case for their one-dimensional solver. It consists of a nearly saturated 1 m high soil column with the parameters presented in Table 1. The initial pore pressure is $h = -20$ cm, meaning that the initial volumetric water content is $\theta=0.323$.

The objective is to validate the solver by checking the mass-conservation as well as the ability of the solver to converge to a hydrostatic equilibrium. The waterflow is simply driven by gravity and the boundaries are waterproof, meaning that no water can flow out of the system.

The present solver provides convincing results as shown in Figure 3, no water enters or flows out of the system and a perfect hydrostatic equilibrium is obtained.

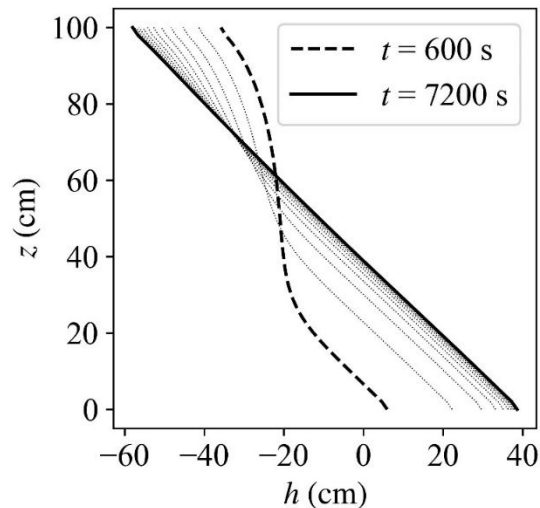


Figure 3 Results of test case 1: Drainage of a soil column

A sharp infiltration front

In this test case, a sharp infiltration front is generated in a soil column by both the initial and the boundary conditions. The initial conditions are described by the following function, where values are expressed in cm:

$$h(x, y, z, t = 0) = \begin{cases} -1000 & \text{if } z > 0.6 \\ -75 - \frac{925}{0.6} & \text{if } 0 \leq z \leq 0.6 \end{cases}$$

Where the z axis is pointing towards the bottom of the column. At the top of the column ($z = 0$ cm), $h = -75$ cm, as at the bottom of the column ($z = 60$ cm) a constant pressure of $h = 1000$ cm is imposed. These results have been used and compared as a benchmark in several articles (Kavetski et al., 2001; Horgue et al., 2015.; Su et al., 2022). Results obtained by Horgue et al. (2015) are used as a reference solution and plotted in dashed lines to compare with the proposed solver. The results obtained with the present method match satisfactorily the reference ones (Figure 4).

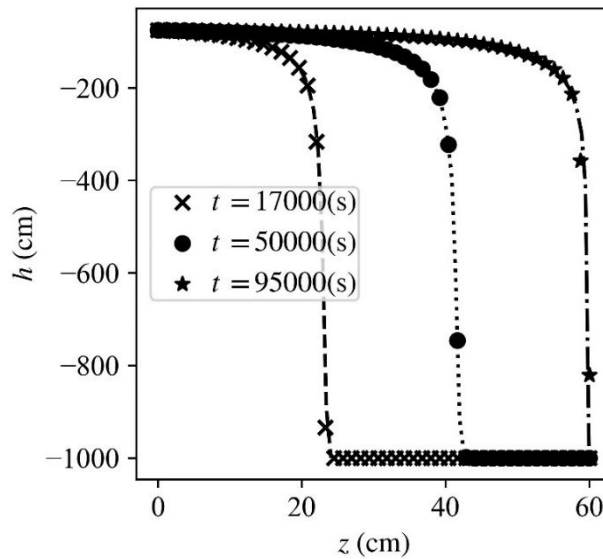


Figure 4 Results of test case 2: Sharp infiltration front. Dashed lines represent the results by Horgue et al. (2015)

3 Coupling between Richards and shallow-water equations

3.1 Spatial and temporal coupling

The shallow water equations are used to describe the flow over the dike. Considering a unit-width system, the equations can be written as:

$$\frac{\partial h}{\partial t} + \frac{\partial q}{\partial x} = q_{in} \quad (11a)$$

$$\frac{\partial q}{\partial t} + \frac{\partial}{\partial x} \left(\frac{q^2}{h} + g \frac{h^2}{2} \right) = g h (S_0 - S_f) \quad (11b)$$

Where h is the water depth (m), $q = uh$ the unit discharge ($\text{m}^2 \cdot \text{s}^{-1}$) with u the depth-averaged velocity, S_0 the bed slope (-) and S_f the friction slope (-) calculated using Manning's friction formulation. Equations (11) are solved using an explicit finite volume scheme with the fluxes at the interfaces evaluated using Roe's scheme (Soares-Frazão, 2007).

Spatial coupling between the Richards and shallow-water equations is achieved at the interface between the two systems, i.e., the embankment surface, using appropriate boundary conditions. Although on site the interface between the subsurface environment and the surface flow domain is not so well defined (silt, sediments, etc.), it is generally considered that this interface is sharp to facilitate the mathematical approach (Furman, 2008). In the present model, as illustrated in Figure 6, the subsurface and the surface cells are perfectly aligned. In this way no interpolation or remapping is required to obtain the boundary information, which avoids error propagation.

The algorithm consists in using the water depth of the surface flow as the boundary condition for the Richards' equation and using the calculated internal flows as source terms q_{in} in the mass conservation equation (11a).

From a temporal point of view, the resolution method is staggered in the sense that the resolution of the shallow-water equations requires small time steps due to the explicit nature of the resolution scheme, whereas the implicit resolution of the Richards' equation allows the use of large time steps without losing too much precision. This time integration scheme is illustrated in Figure 5. In addition, since the flow through the soil is much slower than the free-surface flow, no information is lost with this decoupling.

3.2 Source terms

Considering a unit-width dike as illustrated in Figure 6, the mass-balance is formally established as follows for the source term representing the volume of water infiltrating in the dike $V_{in,i}$ (12):

$$V_{in,i} = \sum_j v_{i,j} L_{i,j} \Delta t + (\theta_i^{n+1} - \theta_i^n) \Omega_i \quad (12)$$

Where v_i denotes the flow velocity between the boundary cell and its adjacent cells evaluated using Darcy's law and L_i is the length of the corresponding interface. The second part of equation (12) takes into account the part of water absorbed by the soil of the cell itself. This volume tends very quickly towards 0 because the boundary cell is saturating almost instantaneously.

Using the definition (12) of the infiltrated volume, let us define the equivalent infiltrated height extracted from the cell of the shallow water domain:

$$\Delta h_{in,i} = \frac{V_{in,i}}{\Delta x_i} = q_{in,i} \Delta t \quad (13)$$

This water height must be removed from the cell at the end of each Richards equation time step and is used to calculate the source term q_{in} of (11a).

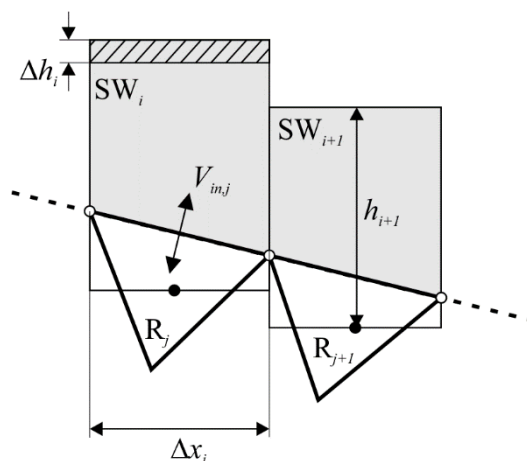


Figure 5 Schematic representation of the mass exchanged between the shallow-water equations cells (SW) and the Richards equation cells (R)

4 Model validation

4.1 Flow through an embankment

Experiments by Ebrahimi et al. (2007) in which they collected an extensive set of data for the study of seepage flows are used to validate the proposed model. The test consists of applying a tidal wave on a sandy embankment. On both sides of the embankment an initial 274 mm water level is initially set. The sand is non-cohesive and has a mean diameter of 1 mm and a hydraulic conductivity of 1 cm s^{-1} . No other soil parameters are provided by Ebrahimi et al. (2007), therefore the general features of the test case are reproduced but the results cannot be compared.

A cyclic tidal wave was applied on one side of the embankment and the objective is to observe its influence on the other side. The tidal wave's equation is the following:

$$z_w(x=0) = 0.214 + 0.06 \cos\left(\frac{2\pi t}{355}\right)$$

The mean water level of the tidal wave is 0.214 m and its amplitude is 0.06 m. A 355 s period is imposed. The water level variation at up and downstream points of the embankment were monitored during the whole process. More technical details about the design of this experimental test case are extensively explained in Ebrahimi et al. (2007).

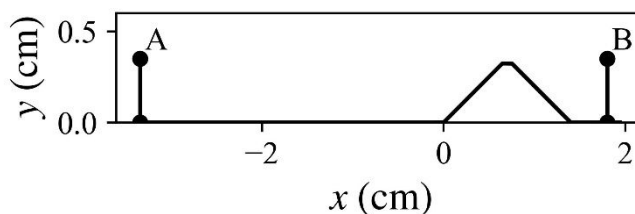


Figure 6 Schematic view of the experimental setup

The computed results are illustrated in Figure 7. It can be observed that after two oscillations, a steady state takes place at the downstream side of the dike (gauge B, $x = 1.8$ m). There is an observable 90° phase lag between the two water surface oscillations. The obtained results with our proposed coupled solver match those observations.

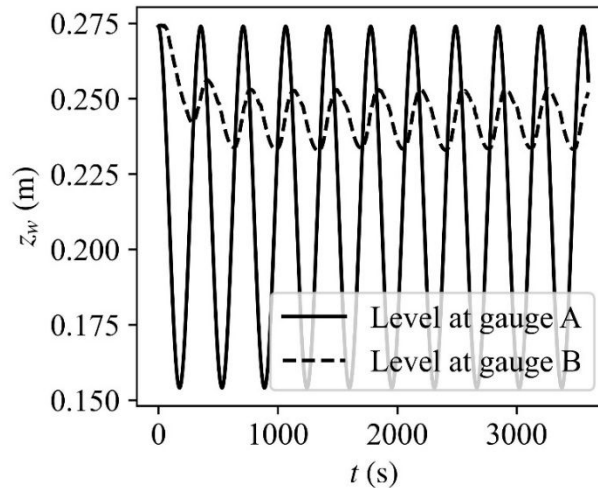


Figure 7 Water level's evolution at both sides of the dike

4.2 Flow through and over embankment: influence of initial water saturation level

The objective of the current test case is to highlight the influence of the initial saturation on the internal pore pressure evolution when the dike is submitted to an overtopping flow.

The dike is 4.5 m wide and 1 m high and its soil has the same parameters as those presented at Table 1, excepted for the hydraulic conductivity set to $K_s = 0.05 \text{ cm s}^{-1}$ and a pore pressure initialized at $h = -40$ cm. Two cases are presented in which the initial water level at the upstream side is 0.75 m. In case (a) a $0.1 \text{ m}^3\text{s}^{-1}$ flow is directly released on the dike while in case (b) the same flow is released only after 500 s. As a result, it can be observed that during the first 500 s a saturation profile is developed from the upstream part to the downstream seepage face. Due to this profile, the steady state is obtained much faster as the unsaturated soil zone is reduced. In figure 8 we can observe the state of pore pressure in the soil 20 s after the release of the flow for case (a) and case (b). The initial water saturation of case (b) enables the water of the overtopping to penetrate much faster in the soil.

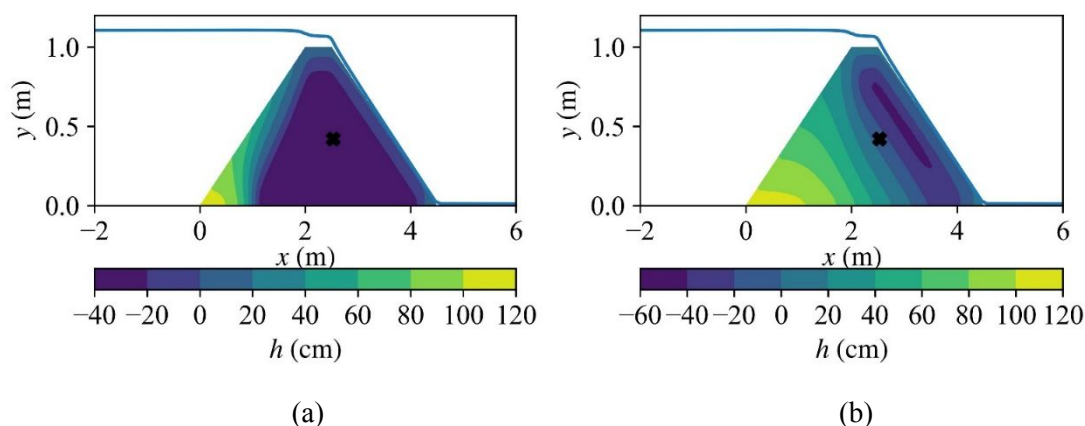


Figure 8 (a) unsaturated dike overtopping, (b) saturated dike overtopping

An observation gauge is chosen at a certain point of the dike ($x = 2.53$ m, $y = 0.42$ m) and is used to compare the evolution of the pore pressure from the start of the overtopping flow in each case.

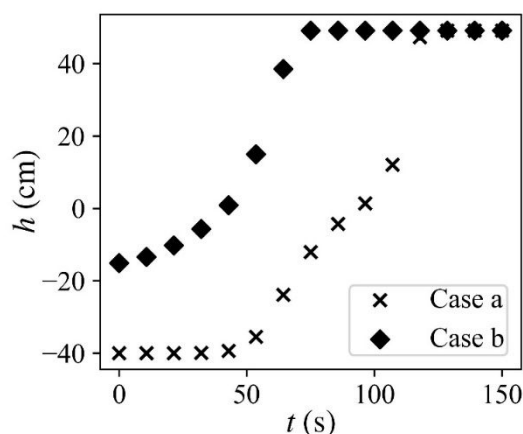


Figure 9 Comparison of the pore pressure evolution from the start of the overtopping

The comparison of the pore pressure values at the gauge emphasizes the importance of the initial soil saturation on the full saturation rate. Indeed, we can observe that the time needed to reach the steady state is two times faster in case of an initially almost saturated dike (b).

As the pore pressure is a key-factor for the strength of the dike, the time needed to reach the full-saturation also appears as a key-factor.

4.3 Flow through and over an embankment

In this section, another test case is presented which examines the impact of different saturated hydraulic conductivities, without changing the other soil parameters, on the groundwater flow and internal pore pressure of an embankment dike when subjected to overtopping flow. At figure 10 (a), the influence of the saturated hydraulic conductivity on the unsaturated hydraulic

conductivity can clearly be identified. As the saturated conductivity is great ($K_s = 1 \text{ cm s}^{-1}$), the soil can be associated to gravels. Values such as $K_s = 0.1 \text{ cm s}^{-1}$ or $K_s = 0.01 \text{ cm s}^{-1}$ can often be associated to sand and lower values ($K_s = 0.001 \text{ cm s}^{-1}$) represent silt.

The test case is conducted on the same geometry as the previous test case (illustrated in Figure 8) and the same overtopping flow is released. The results, as shown in Figure 10 (b), clearly demonstrate the significant influence of hydraulic conductivity on the infiltration rate and internal pore pressure of the dike. The steady state is reached when all available volume in the pores of the soil is filled with water.

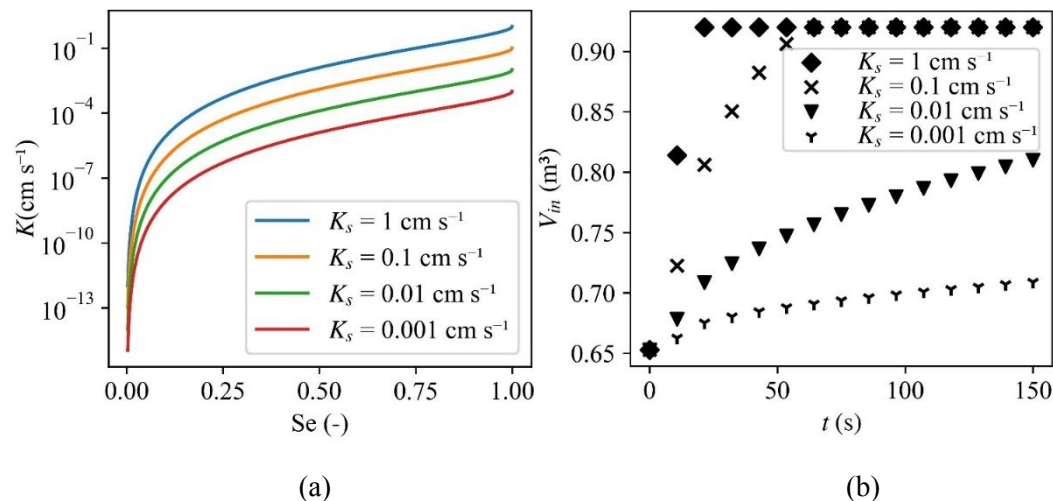


Figure 10 (a) Comparison of the unsaturated hydraulic conductivities (b) Comparison of infiltrated water volume

Given that the dike is fully submerged under water, there is no means for water to escape, making the infiltration rate and internal pore pressure particularly crucial for the stability of the structure. A higher hydraulic conductivity results in faster infiltration and a more significant impact on the internal pore pressure in the short-term. These findings are of great importance for the design and construction of dikes, particularly for clay core and clay surface dikes, as the hydraulic conductivity of the soil must be closely considered to ensure the stability and safety of the structure.

5 Conclusion

In this article a new coupled solver for the numerical calculation of sub-surface and the surface flows on unstructured meshes was presented.

At first, we developed and validated a new finite volume scheme for solving the Richards equation which appeared to be efficient and precise. The latter was validated against classical benchmarks, such as the drainage of a soil column or a sharp infiltration front. The simplicity

1
2
3 of the formulation but also its ability to solve the equation in the saturated as well as in the
4 unsaturated zone renders the solver very interesting for further applications.

5
6 The subsurface flow was linked to the surface flow via a source term which allows to respect
7 the mass conservation. The resulting solver appears to be effective and allows to understand
8 how the interaction between the surface and subsurface flows and the soil characteristics could
9 affect the internal flow and the evolution of the degree of saturation of the dike, which is a key
10 parameter in dike stability assessment. We emphasized the importance of the initial saturation
11 level but also of the saturated hydraulic conductivity on the time needed to reach the steady
12 state.
13

14
15 The new solver proved to be efficient in different types of test cases involving complex
16 combinations of flows. Future work will be dedicated to the validation of the solver by
17 comparison with experimental data.
18
19
20
21
22
23
24
25
26
27
28
29
30
31
32
33
34
35
36
37
38
39
40
41
42
43
44
45
46
47
48
49
50
51
52
53
54
55
56
57
58
59
60

6 Notation

θ = volumetric water content (-)

θ_s = saturated volumetric water content (-)

θ_r = residual volumetric water content (-)

S_e = equivalent volumetric water content (-)

K = hydraulic conductivity (cm s^{-1})

K_s = saturated hydraulic conductivity (cm s^{-1})

α = parameter linked to the air-entry pressure (cm^{-1})

η = parameter linked to the distribution of the pores in the soil (Mualem-van Genuchten model)

L = parameter of the Mualem-van Genuchten model (-)

μ = parameter of the Mualem-van Genuchten model (-)

h = pressure (cm)

h_e = pore entry pressure (cm)

Δt = time step (s)

Ω_i = cell area in the Richards domain's (m^2)

L_{ij} = length of the specific edge between i and j (cm)

n_z = outgoing z -axis pointing normal (-)

h = water depth (m)

q = unit discharge ($\text{m}^2 \text{s}^{-1}$)

g = gravity (m s^{-2})

S_0 = bed slope (-)

S_f = friction slope (-)

7 References

Benson, C., Chiang, I., Chalermyanont, T., & Sawangsuriya, A. (2014). *Estimating van Genuchten Parameters α and n for Clean Sands from Particle Size Distribution Data*. 410-427. <https://doi.org/10.1061/9780784413265.033>

Casulli, V. (2017). A coupled surface-subsurface model for hydrostatic flows under saturated and variably saturated conditions : A coupled surface-subsurface model for hydrostatic flows. *International Journal for Numerical Methods in Fluids*, 85(8), 449-464. <https://doi.org/10.1002/fld.4389>

- 1
2
3 Caviedes-Voullième, D., Garcí'a-Navarro, P., & Murillo, J. (2013). Verification,
4
5 conservation, stability and efficiency of a finite volume method for the 1D Richards
6
7 equation. *Journal of Hydrology*, 480, 69-84.
8
9 <https://doi.org/10.1016/j.jhydrol.2012.12.008>
10
11 Caviedes-Voullième, D., Murillo, J., & Garcia-Navarro, P. (2012, juin 1). *Numerical*
12
13 *simulation of groundwater- surface interactions by external coupling of the 3D*
14
15 *Richards equation and the full 2D shallow-water equations.*
16
17
18 Celia, M. A., Bouloutas, E. T., & Zarba, R. L. (1990). A general mass-conservative numerical
19
20 solution for the unsaturated flow equation. *Water Resources Research*, 26(7),
21
22 1483-1496. <https://doi.org/10.1029/WR026i007p01483>
23
24 Chávez-Negrete, C., Domínguez-Mota, F. J., & Santana-Quinteros, D. (2018). Numerical
25
26 solution of Richards' equation of water flow by generalized finite differences.
27
28 *Computers and Geotechnics*, 101, 168-175.
29
30 <https://doi.org/10.1016/j.compgeo.2018.05.003>
31
32
33 De Maet, T., & Hanert, E. (2011). *An explicit Discontinuous-Galerkin surface-subsurface*
34
35 *water flow model*. Fifth International Conference on Advanced COmputational
36
37 Methods in ENgineering (ACOMEN 2011).
38
39 <https://dial.uclouvain.be/pr/boreal/object/boreal:107584>
40
41 Ebrahimi, K., Falconer, R. A., & Lin, B. (2007). Flow and solute fluxes in integrated wetland
42
43 and coastal systems. *Environmental Modelling & Software*, 22(9), 1337-1348.
44
45 <https://doi.org/10.1016/j.envsoft.2006.09.003>
46
47
48 Farthing, M. W., & Ogden, F. L. (2017). Numerical Solution of Richards' Equation : A
49
50 Review of Advances and Challenges. *Soil Science Society of America Journal*, 81(6),
51
52 1257-1269. <https://doi.org/10.2136/sssaj2017.02.0058>
53
54 Foster, M., Fell, R., & Spannagle, M. (2000). The statistics of embankment dam failures and
55
56 accidents. *Canadian Geotechnical Journal*, 37(5), 1000-1024.
57
58 <https://doi.org/10.1139/t00-030>
59
60

- 1
2
3 Furman, A. (2008). Modeling Coupled Surface–Subsurface Flow Processes : A Review.
4
5 *Vadose Zone Journal*, 7, 741. <https://doi.org/10.2136/vzj2007.0065>
6
7 Horgue, P., Franc, J., Guibert, R., & Debenest, G. (s. d.). *An extension of the open-source*
8
9 *porousMultiphaseFoam toolbox dedicated to groundwater flows solving the*
10
11 *Richards' equation*.
12
13 Kavetski, D., Binning, P., & Sloan, S. W. (2001). Adaptive time stepping and error control in
14
15 a mass conservative numerical solution of the mixed form of Richards equation.
16
17 *Advances in Water Resources*, 24(6), 595-605. <https://doi.org/10.1016/S0309->
18
19 1708(00)00076-2
20
21 Mizutani, H., Nakagawa, H., Yoden, T., Kawaike, K., & Zhang, H. (2013). Numerical
22
23 modelling of river embankment failure due to overtopping flow considering
24
25 infiltration effects. *Journal of Hydraulic Research*, 51(6), 681-695.
26
27 <https://doi.org/10.1080/00221686.2013.812151>
28
29 Mualem, Y. (1976). A new model for predicting the hydraulic conductivity of unsaturated
30
31 porous media. *Water Resources Research*, 12(3), 513-522.
32
33 <https://doi.org/10.1029/WR012i003p00513>
34
35 Richards, L. A. (1931). Capillary conduction of liquids through porous mediums. *Physics*,
36
37 1(5), 318-333. <https://doi.org/10.1063/1.1745010>
38
39 Shao, S., Ji, C., Graham, D. I., Reeve, D. E., James, P. W., & Chadwick, A. J. (2006).
40
41 Simulation of wave overtopping by an incompressible SPH model. *Coastal*
42
43 *Engineering*, 53(9), 723-735. <https://doi.org/10.1016/j.coastaleng.2006.02.005>
44
45 Shiach, J., Mingham, C. G., Ingram, D., & Bruce, T. (2004). The applicability of the shallow
46
47 water equations for modelling violent wave overtopping. *Coastal Engineering*, 51,
48
49 1-15. <https://doi.org/10.1016/j.coastaleng.2003.11.001>
50
51 Soltani, A., Azimi, M., Boroomandnia, A., & O'Kelly, B. C. (2021). An objective framework
52
53 for determination of the air-entry value from the soil–water characteristic curve.
54
55 *Results in Engineering*, 12, 100298. <https://doi.org/10.1016/j.rineng.2021.100298>
56
57
58
59
60

- 1
2
3 Su, X., Zhang, M., Zou, D., Zhao, Y., Zhang, J., & Su, H. (2022). Numerical scheme for
4 solving the Richard's equation based on finite volume model with unstructured mesh
5 and implicit dual-time stepping. *Computers and Geotechnics*, *147*, 104768.
6
7 <https://doi.org/10.1016/j.compgeo.2022.104768>
8
9
10
11 Tsai, T.-L., Chen, H.-E., & Yang, J.-C. (2008). Numerical modeling of rainstorm-induced
12 shallow landslides in saturated and unsaturated soils. *Environmental Geology*, *55*(6),
13 1269-1277. <https://doi.org/10.1007/s00254-007-1075-1>
14
15
16
17 Van Emelen, S., Zech, Y., & Soares-Frazão, S. (2016). Closure to “Impact of sediment
18 transport formulations on breaching modelling” by S. VAN EMELEN, Y. ZECH and
19 S. SOARES-FRAZÃO, J. Hydraulic Res. *53*(1), 2015, 60–72. *Journal of Hydraulic*
20 *Research*, *54*, 481-483. <https://doi.org/10.1080/00221686.2016.1199054>
21
22
23
24
25
26
27 Van Genuchten, M. (1980). A Closed-form Equation for Predicting the Hydraulic
28 Conductivity of Unsaturated Soils I. *Soil Science Society of America Journal*, *44*.
29 <https://doi.org/10.2136/sssaj1980.03615995004400050002x>
30
31
32
33 Weill, S., Mouche, E., & Patin, J. (2009). A generalized Richards equation for
34 surface/subsurface flow modelling. *Journal of Hydrology*, *366*(1), 9-20.
35 <https://doi.org/10.1016/j.jhydrol.2008.12.007>
36
37
38
39
40
41
42
43
44
45
46
47
48
49
50
51
52
53
54
55
56
57
58
59
60

1
2
3 **List of tables**
4

5
6 Table 1 Soil parameters for the test cases
7
8
9
10
11
12
13
14
15
16
17
18
19
20
21
22
23
24
25
26
27
28
29
30
31
32
33
34
35
36
37
38
39
40
41
42
43
44
45
46
47
48
49
50
51
52
53
54
55
56
57
58
59
60

List of figures

Figure 1 Schematic representation of the soil-water retention curve

Figure 2 Computational cells for the Richards equation, definition of variables.

Figure 3 Results of test case 1: Drainage of a soil column

Figure 4 Results of test case 2: Sharp infiltration front. Dashed lines represent

Figure 5 Schematic representation of the mass exchanged between the shallow-water equations cells (SW) and the Richards equation cells (R)

Figure 6 Schematic view of the experimental setup

Figure 7 Water level's evolution at both sides of the dike

Figure 8 (a) unsaturated dike overtopping, (b) saturated dike overtopping

Figure 9 Comparison of the pore pressure evolution from the start of the overtopping

Figure 10 (a) Comparison of the unsaturated hydraulic conductivities (b) Comparison of infiltrated water volume